



Synthesis of Fe₃O₄ magnetic nanoparticles coated with cationic surfactants and their applications in Sb(V) removal from water

Wenjing Guo^{a,b}, Zhiyou Fu^{a,*}, Zhiyong Zhang^b, Hao Wang^c, Shasha Liu^a, Weiyong Feng^a, Xiaoli Zhao^a, John P. Giesy^{a,d}

^a State Key Laboratory of Environment Criteria and Risk Assessment, Chinese Research Academy of Environmental Sciences, Beijing 100012, China

^b Institute of Agricultural Resource and Environmental Sciences, Jiangsu Academy of Agricultural Sciences, Nanjing 210014, China

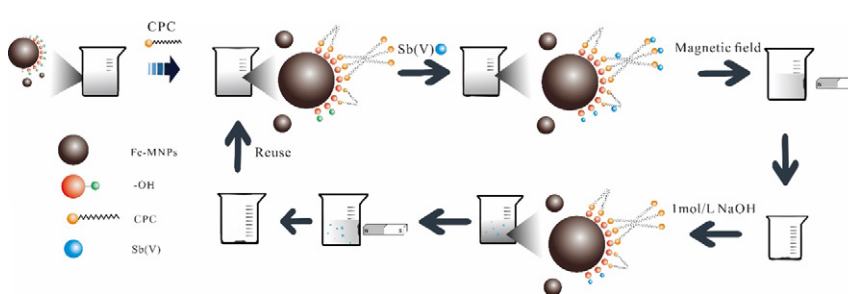
^c South China Institute of Environmental Sciences, Ministry of Environmental Protection, Guangzhou 510655, China

^d Department of Biomedical and Veterinary Biosciences and Toxicology Centre, University of Saskatchewan, Saskatoon, Saskatchewan, Canada

HIGHLIGHTS

- Sb(V) removal by Fe-MNPs coated with CPC was better than that with CTAB.
- Removal ability of the adsorbent was superior than several traditional adsorbents.
- Electrostatic attraction and surface bonding contribute Sb(V) removal mechanisms.

GRAPHICAL ABSTRACT



ARTICLE INFO

Article history:

Received 3 September 2019

Received in revised form 3 December 2019

Accepted 21 December 2019

Available online 26 December 2019

Editor: Ching-Hua Huang

Keywords:

Fe₃O₄

Magnetic nanoparticle

Adsorption

Sb(V)

Surfactant

ABSTRACT

Antimony (Sb) pollution was an emerging environmental risk in several contaminated waters, whereas its removal still presented as a severe challenge due to the lack of efficient adsorbent and its further removal mechanism. In this study, synthesized adsorbents, Fe₃O₄ magnetic nanoparticles (Fe-MNPs) modified and dispersed with commonly used cationic surfactants, were applied to remove Sb contamination in real surface waters, its synthesized conditions, removal performance and mechanism were investigated by using batch experiments and characterization analyses. Optimum conditions on Sb(V) (the dominant form is Sb(OH)₆⁻) removal by modified adsorbents were obtained as: cetylpyridinium chloride (CPC) coated on Fe-MNPs, mass ratio of Fe-MNPs:CPC = 4:1 and pH = 3–5. Magnetic properties of synthesized adsorbent were not affected, dispersibility was enhanced after fabrication of CPC, that indicated the Fe-MNPs@CPC could be separated and reused with external magnetic field. The adsorption efficiency of this low-cost adsorbent coated with CPC was superior than several traditional adsorbents. The practical application of Fe-MNPs@CPC in five types real waters from the Xikuangshan (XKS) Sb mine area and regeneration experiments by 1 M (mol/L) NaOH solution further confirm its practicability and reusability. Removal experiment results, X-ray photoelectron spectroscopy (XPS) and Fourier transform infrared spectroscopy (FT-IR) spectra suggested that electrostatic attraction and surface bonding might responsible for the Sb(V) removal by Fe-MNPs modified with cationic surfactants.

© 2019 Elsevier B.V. All rights reserved.

* Corresponding author.

E-mail address: zhiyoufu@126.com (Z. Fu).

1. Introduction

As a nonessential emerging metalloid contaminant, antimony (Sb) has received much attention in recent years owing to its widespread application in modern industrial systems, such as batteries, flame retardants, semiconductors, and alloys (Amarasiriwardena and Wu, 2011; Filella et al., 2002a, 2002b). Increased exploitation and usage of Sb have resulted in the uncontrolled release of its compounds into the environment. Thus, elevated concentrations of Sb in environmental media beyond background concentrations have been detected (He et al., 2012; Wu et al., 2011). In surface water, high concentrations of Sb (mg/L level) were measured nearby mine areas and industrial waste (Guo et al., 2018; Liu et al., 2010; Van Velzen, 1998; Watanabe et al., 1999; Fu et al., 2010). Medical evidences have showed that inhalation of Sb can cause damage to the respiratory system, liver, and skin (Gebel et al., 1997; Sundar and Chakravarty, 2010; Guo et al., 2016). In addition, Sb may also be carcinogenic to humans (Hammel et al., 2000; Poon et al., 1998). Thus, Sb compounds have been listed as priority pollutants interest by the European Union (EU) and Environmental Protection Agency of the United States (USEPA) (EU, 1976; USEPA, 1979). Consequently, maximum permissible concentrations of Sb in water have been adopted by many countries and organizations, such as China (5 µg/L in surface water according to GB3838-2002 (SAC, 2002)), USEPA (6 µg/L in drinking water), and the World Health Organization (WHO) (20 µg/L in drinking water). Therefore, there is urgent need to develop an effective strategy for Sb removal from water experiencing heavy pollution.

Several removal strategies, including adsorption (Ungureanu et al., 2015; Vithanage et al., 2015; Wu et al., 2012; Zou et al., 2016), coagulation (Guo et al., 2009; Song et al., 2018; Wu et al., 2010), reverse osmosis (Kang et al., 2000) and electrodeposition (Zhu et al., 2011) have been applied to remove Sb from waters. Of all the removal techniques, adsorption is regarded as a promising method due to its easy-operation, low-cost, and minimal sludge production. Recently, several newly emerging adsorbents, such as nanoscale zero-valent iron (Zhao et al., 2014), graphene oxide (Zou et al., 2016), MnO₂ nanofibers (Luo et al., 2017), and carbon nanofibers (Luo et al., 2015) have been utilized to remove Sb(V) or Sb(III) due to their large capacities for adsorption. However, application of these abovementioned efficient materials might be limited by difficulty in recovery/reuse for their small sizes in aquatic environments (White et al., 2009). Thus, several studies on removal of contaminants have focused on application and regeneration of magnetic adsorbents, for instance, magnetic Fe₃O₄ nanoparticles (MNPs) and γ-Fe₂O₃ nanoparticles that can be easily separated with external magnetic field (Jin et al., 2012; Lin et al., 2012). On the other hand, surfaces of nanoparticles coating with surfactants, functional groups or coupling agents were considered that could avoid their oxidation and aggregation thus improving the dispersibility and removal ability in waters (Chen et al., 2012; Feng et al., 2012). For instance, arsenic(As) and perchlorate removal by Fe₃O₄ superparamagnetic nanoparticles coated with ascorbic acid and granular activated carbon (GAC) modified with cetyltrimethyl ammonium chloride (GAC-CTAC) respectively were achieved in previous studies (Feng et al., 2012; Xu et al., 2011). The abovementioned studies, of which adopted adsorbents surfaces were coated with surfactants to remove contaminants, suggested that magnetic nanoparticles surfaces of which coated with surfactant might be a reusable, efficient and easily separated method for the removal of several contaminants in waters. However, Sb removal on modified magnetite nanoparticles has never been explored so far. Furthermore, adsorption mechanisms of As/Sb on metal adsorbents have gain much in-depth understanding in recent periods (Grossl et al., 1997; Guo et al., 2014), while the adsorption process of these contaminants by adsorbent with introducing of surfactants is still unclear.

In the present study, Sb(V) was selected as targeted contaminant, since this Sb species was more mobile and difficult to be removed, and Sb(V) was dominant Sb species for the rapid oxidation of Sb(III) in

real waters (Filella et al., 2002a; Kong et al., 2016; Leuz and Johnson, 2005). Fe₃O₄ magnetic nanoparticles (Fe-MNPs) coated with cationic surfactants were synthesized as an adsorbent for Sb(V) removal from contaminated water. The main objectives of this study were to (1) investigate optimum cationic surfactants, synthesized conditions and pH ranges, (2) conduct material characterization analysis and removal performance of synthesized adsorbent, including adsorption kinetics/equilibrium, practical application in real contaminated water, and regeneration of adsorbent with various desorbents, finally (3) investigate removal mechanism of Sb(V) by Fe-MNPs when cationic surfactant was introduced based on experiment results and characterization analyses.

2. Materials and methods

2.1. Chemical reagents

CPC was purchased from Alfa Aesar Chemical Co. Ltd. (Tianjin, China); cetyltrimethylammonium bromide (CTAB), ferric chloride (FeCl₃·6H₂O), ferrous chloride (FeCl₂·4H₂O), and sodium hydroxide (NaOH) were purchased from Sinopharm Chemical Reagent (Shanghai, China); Suwannee River humic acid was procured from the International Humic Substances Society (IHSS, Colorado, USA). All other chemicals and reagents used in this study were of analytical-reagent grade or greater purity and purchased from Beijing Chemical Works. De-ionized water used in this study was obtained from a Milli-Q system.

2.2. Preparation of adsorbents

Modified adsorbents were synthesized according to the two-step process of fabrication that has been previously published (Tie et al., 2006; Wang et al., 2006), including preparation of the magnetic Fe₃O₄ nanoparticles and modification of surfaces with surfactants of Fe-MNPs. First, 2.0 g of FeCl₂, 5.2 g of FeCl₃ and 0.85 mL HCl (12 mol/L) were mixed in 25 mL deoxygenated water, which had been degassed with ultrapure nitrogen gas during the synthesis. The mixed solution was added dropwisely into 250 mL of 1.5 mol/L NaOH solution under N₂ protection and continuous stirring at 430–440 rpm. Then, the obtained precipitate was separated by an external magnetic field and washed with 200 mL deionized water to remove Na⁺ in solution.

The acquired precipitate was re-dispersed into 220 mL of certain surfactant (CTAB/CPC) with ultrasonication for 30 min. After this process, synthesized Fe-MNPs were separated and washed with deionized water again, then the obtained black precipitate was dry at 50 °C for 24 h. Fe-MNPs@CPC were stored in a pre-cleaned bottle for the batch experiments and characterization within a month.

2.3. Characterizations of adsorbent

Elemental compositions of samples were characterized by use of XPS (PHI Quantera SXM, ULVAC-PHI, Japan), with amonochromated X-ray beam (100 µm) from an Al target at an angle of 45°. Binding energy was calibrated with C 1s of 284.8 eV. Functional groups of coated Fe-MNPs were determined by FT-IR (Nicolet iS5, Thermo Scientific, Massachusetts, USA) by use of the KBr disk method. Sizes and morphology of Fe-MNPs coated with surfactants were observed by TEM (Transmission electronic microscopy) (H-7500, Hitachi, Japan); Magnetic properties were obtained by magnetometer (BKT-4500Z, Quantum Design, US) at room temperature (25 ± 1 °C). XRD (X-ray diffraction) patterns of adsorbents were obtained by using XRD analysis (D8 advance, Bruker, Germany).

2.4. Batch adsorption experiments

Adsorption kinetics experiments were conducted in 50 mL pre-cleaned tubes at room temperature of 25 ± 1 °C. The 0.4 g/L of Fe-

MNPs coated with surfactants and pure Fe-MNPs were dispersed into 40 mL synthesized water containing Sb(V), then the tubes were stirred in shaking tables at 100 rpm for sufficient time. Approximately 1 mL aliquot was taken from suspension in assigned time points for determination of Sb(V). The acidic and alkaline conditions were set as 3.0 ± 0.1 and 11.0 ± 0.1 , respectively.

The mass ratio of Fe-MNPs and surfactant and pH of adsorption systems were also investigated to obtain optimum conditions for Sb(V) removal. Initial Sb(V) concentrations ranged from 2 to 25 mg/L and 0.4 g/L of adsorbent were added into solutions to obtain adsorption isotherms. Effect of several competitive matters, including nitrate, sulfate, phosphate and humic acid (HA), were also determined by added different contents of these matters into removal systems.

Adsorbent was applied to remove Sb(V) in typical contaminated waters, which included paddy field water, reservoir water, tap water, retained water and well water. These real waters were collected from the Xikuangshan (XKS) Sb mine (Hunan Province, China), which is one of the world's major producers of Sb and renowned as the "World's Antimony Capital" (He et al., 2012). Removal experiments on real waters were following the same procedure as described in batch experiments.

2.5. Regeneration and reuse of adsorbent

Various desorption solutions, including deionized water, different concentrations of NaOH solutions and EDTA-2Na (chelating agent) solution that applied in the previous study as desorbent (Leng et al., 2012; Li et al., 2011), were compared to evaluate the regeneration performance of adsorbents through five consecutive adsorption/desorption cycles. For each consecutive cycle, 0.4 g/L adsorbent was added to a solution containing 1 mg/L Sb(V). After adsorption was completed, 40 mL of various desorption solutions were added to tubes and rotated at 100 rpm for 12 h, then, deionized water was used to wash adsorbents three times. Adsorbents were then separated for use in subsequent adsorption/desorption cycles.

2.6. Analytical methods

Concentrations of Sb(V) in solutions were measured by use of Hydride Generation-Atomic Fluorescence Spectrometry (HG-AFS, Millennium Excalibur System, Kent, UK). Conditions for the HG-AFS were same as described in previous study (Guo et al., 2018). ζ potential of adsorbents in aqueous solution was measured by use of a Zetasizer Nano meter (Malvern, England).

3. Results and discussion

3.1. Optimum conditions on Sb(V) adsorption

3.1.1. Different surfactants coated on Fe-MNPs

Cationic surfactants (CPC or CTAB) were coated onto surfaces of Fe₃O₄ magnetic nanoparticles to synthesize adsorbents. pH of removal systems containing 2 mg/L Sb(V) were adjusted to evaluate the removal performance of these adsorbents. As presented in Fig. 1, pure Fe-MNPs and two surfactants coated with surfactants resulted to the different removal performance in pH range of 2–12. Pure Fe-MNPs and Fe-MNPs@CTAB exhibited higher removal percentages under acidic conditions, but lower removal percentages under more alkaline conditions. While Fe-MNPs@CPC exhibited relatively high removal under alkaline conditions. For instance, removal rate of Sb(V) in the presence of pure Fe-MNPs was 6.25% at pH = 11.04, Fe-MNPs@CTAB was 12.8% at pH = 10.0, for Fe-MNPs@CPC, removal rate was still reached 80.2% when pH = 10.1.

Zeta potentials of pure Fe-MNPs, Fe-MNPs@CTAB and Fe-MNPs@CPC were measured to interpret the difference of removal performance over a range of pH (Fig. S1). Compared with surface charge of bare Fe-MNPs, the modification of surfactants increased the zeta potential remarkably

in the wide pH range of 2–12. With the addition of surfactants, the surface charge of adsorbent was altered from electronegative to electropositive through the bonding of cation surfactants with deprotonated —OH groups, similar results also were found in previous study (Zhao et al., 2008). Zeta potentials of two adsorbents coated with CPC and CTAB exhibited similar trends as a function of pH. The positive charge on surfaces of Fe-MNPs@CPC was more than that of Fe-MNPs@CTAB, especially under alkaline conditions, which could explain the greater removal rate of former adsorbent (Fig. 1). Therefore, CPC was selected as the surfactant in this study, with which to coat surfaces of Fe-MNPs.

XPS spectra of various samples showed that the processes of Sb(V) removal by Fe-MNPs@CPC was different from that of Fe-MNPs@CTAB. At acidic condition, Sb 3d_{3/2} peaks of Fe-MNPs@CPC and Fe-MNPs@CTAB (Fig. 2a and c) corresponded to the surface bonding of Sb(V) with nanoscale adsorbents. At alkaline condition, Sb 3d_{3/2} peaks were observed when Sb(V) was adsorbed to Fe-MNPs@CPC (Fig. 2b), while no peak was observed for Fe-MNPs@CTAB (Fig. 2d). The different spectra indicated that surface complexation was involved in the adsorption of Sb(V) by Fe-MNPs@CPC at higher pH. This result could explain the difference in adsorption performance of these two adsorbents under alkaline conditions. Overall, the removal rate of Sb(V) by Fe-MNPs@CPC can be attributed to the larger, positive zeta potential and surface bonding with Sb(OH)₆⁻ on surfaces of adsorbent.

3.1.2. Optimum mass ratio and pH conditions

Results of previous studies revealed that self-assembly of surfactants on surfaces of Fe₃O₄ MNPs could be divided into three phases: hemimicelles, mixed hemimicelles, and admicelles (Atkin et al., 2003; Zhao et al., 2008), and different phases could result in different removal performances. To investigate the optimum conditions for Sb(V) removal, various amounts of Fe-MNPs and CPC in acidic and alkaline conditions were tested to determine optimal conditions for Sb(V) removal. The results in Fig. 3 showed that the mass ratio of 4:1 (Fe-MNPs: CPC) could maximize removal of Sb(V) under either acidic or alkaline conditions. A similar mass ratio (3.3:1), which was observed previously for similar materials (Zhao et al., 2008), was likely due to a corresponding optimum removal efficiency of hemimicelles and mixed hemimicelles. In hemimicelles phases, surfactant anchored with deprotonated —OH groups on the surface of Fe-MNPs and forming surfactant monolayer. With the addition of CPC, surfactant bilayer could be formed which driven by hydrophobic interactions of long chain alkanes in mixed hemimicelles phase. Herein, the Fe-MNPs and CPC ratio of 4:1 were applied in the batch experiments.

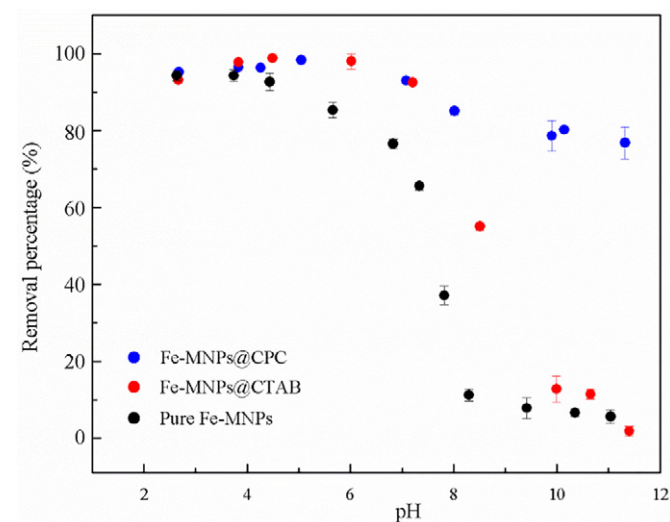


Fig. 1. Removal rates by Fe-MNPs@CPC, Fe-MNPs@CTAB and pure Fe-MNPs in pH of 2–12. (Initial adsorbent concentration: 0.4 g/L; Sb(V) concentration: 2 mg/L; temperature: 25 ± 1 °C).

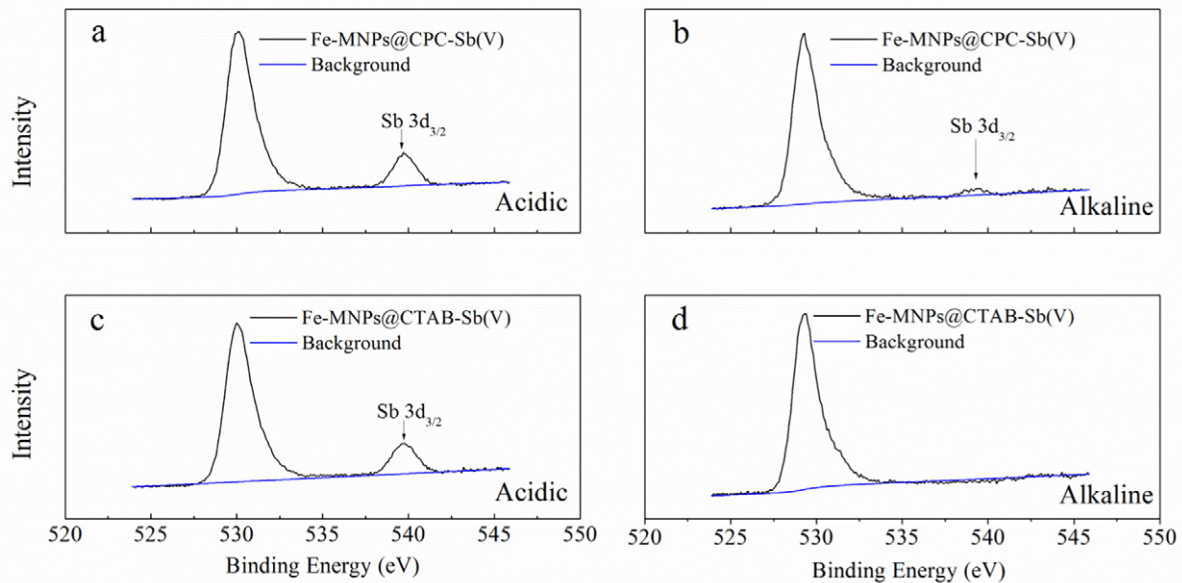


Fig. 2. XPS spectra of Fe-MNPs@CPC (a and b) and Fe-MNPs@CTAB (c and d) loading with Sb(V) under acidic or alkaline conditions.

Various pH conditions were adjusted to evaluate adsorption of Sb(V) with Fe-MNPs@CPC. The results presented in Fig. S2 showed that optimum rates of removal were achieved in the range of pH of 3–5, and the highest removal percentage of 96.8% was observed at a pH of 4.3. Removal of Sb(V) decreased gradually with increased pH, reaching 80.1% in pH of 8.9. The decreasing removal rate at higher pH can be attributed to more negative charges adsorbents carried under alkaline conditions that could compete with $\text{Sb}(\text{OH})_6^-$.

3.2. Property and adsorption performance of Fe-MNPs@CPC on Sb removal

3.2.1. Characterization of Fe-MNPs@CPC

TEM images of bare Fe-MNPs, synthesized Fe-MNPs@CPC and Fe-MNPs@CPC loaded with Sb(V) showed that mean sizes of particles of these materials were 5–10 nm (Fig. 4 a, b and c). These results indicated that modification of CPC didn't alter morphology or microstructure of these types of nanoparticles. TEM images also showed that coating surfaces with CPC enhanced dispersibility and inhibited aggregation of the nanoscale particles (Fig. 4b and c) compared with morphology characteristic of bare Fe-MNPs (Fig. 4a).

This newly coated adsorbents presented superparamagnetic properties in Sb(V) removal. Hysteresis was not observed in this study, and the remanence and coercivity were zero, indicating that this adsorbent respond magnetically in the presence of external magnetic field, and responds rapidly when the magnetic field was removed. Saturation magnetization curves of Fe-MNPs@CPC showed that large saturation magnetization reached 48 emu/g at room temperature (Fig. 4d). This saturation magnetization of coated Fe-MNPs was slightly lower than that of bare Fe-MNPs, which was synthesized by the same process in a previous study (Zhao et al., 2008), but higher than the saturation magnetization of 40 emu/g for Fe_3O_4 nanoparticles coated with ascorbic acid (Feng et al., 2012) and 14.82 emu/g for Fe_3O_4 nanoparticles that prepared by the standard hydrothermal method (Sun et al., 2008). This result suggested that the nanoparticles were susceptible to external magnetic field and this coated adsorbent could be separated easily in real Sb(V) removal.

A total of six peaks in XRD patterns of different samples (Fig. S3) corresponded to peaks characteristic of pure Fe_3O_4 (JCPD standards: Fe_3O_4 , 89–3854, $2\theta = 30.088, 35.439, 43.07, 53.432, 56.958, \text{ and } 62.546$). These similarities among XRD patterns indicated that crystal

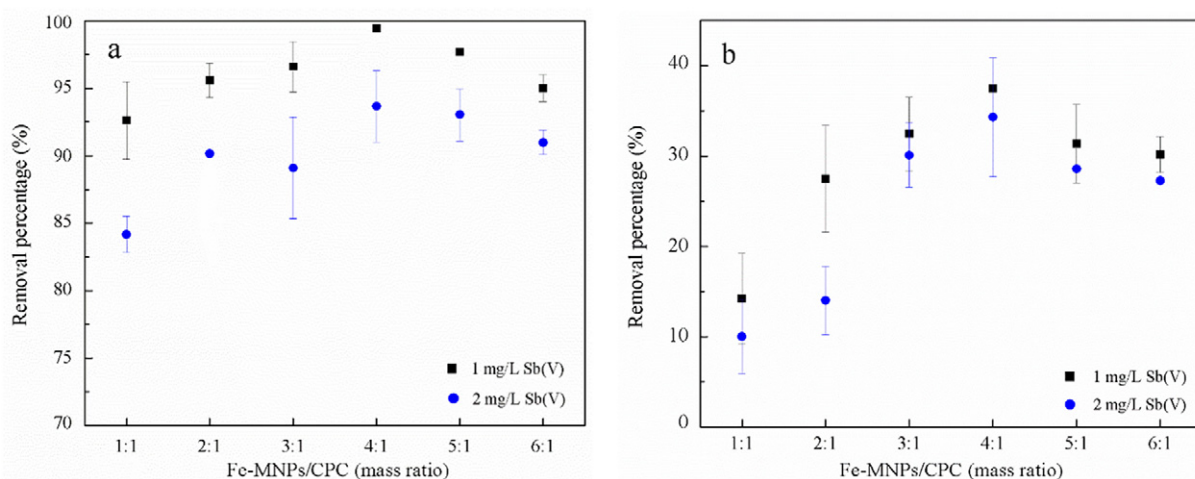


Fig. 3. Effects of amounts of Fe-MNPs and CPC under (a) acidic conditions and (b) alkaline conditions. Initial adsorbents concentration was 0.6 mmol CPC/L; temperature: 25 ± 1 °C.

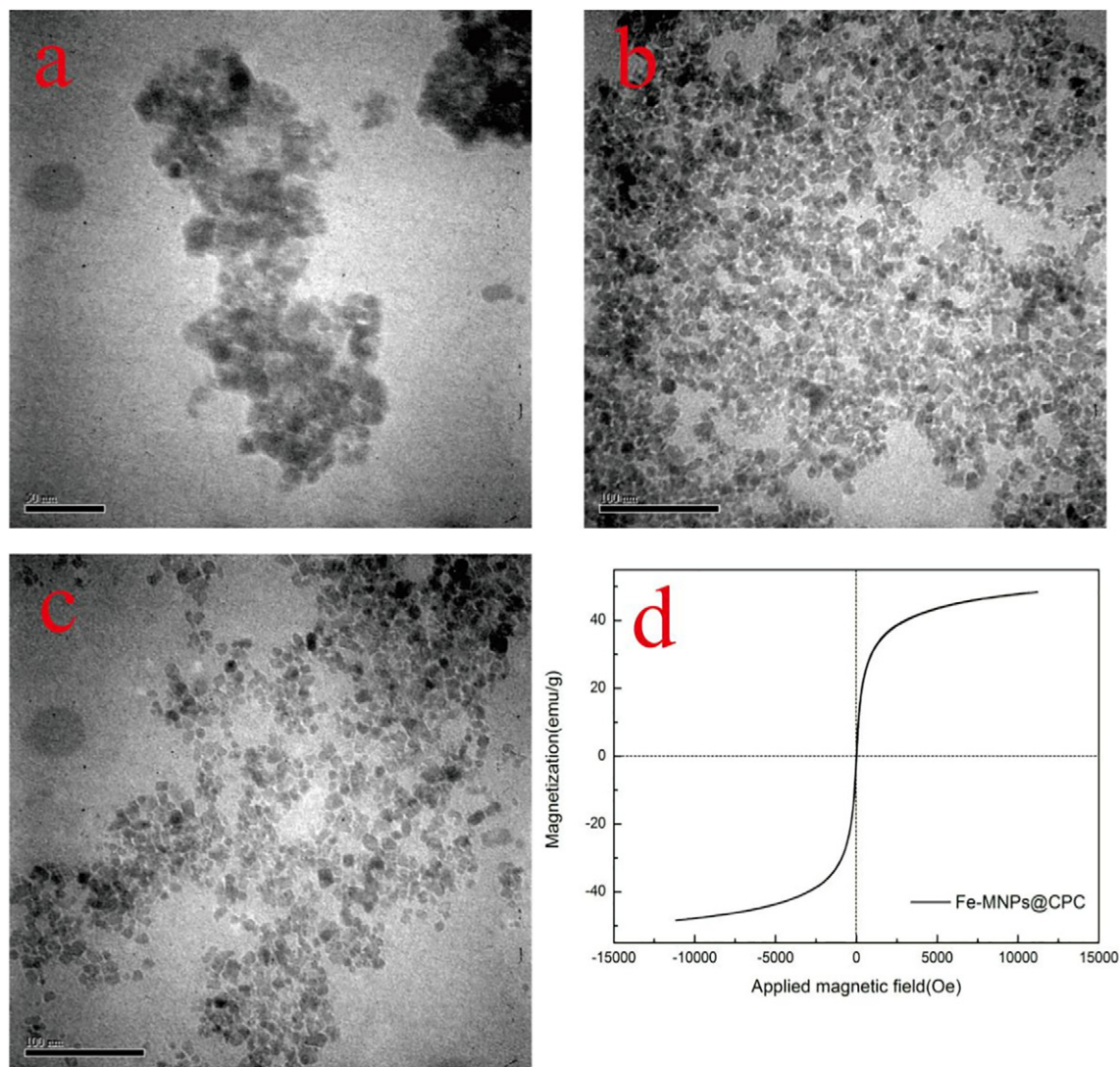


Fig. 4. TEM images of (a) bare Fe-MNPs, (b) synthesized Fe-MNPs@CPC, (c) Fe-MNPs@CPC loaded with Sb(V), (d) magnetization curves of Fe_3O_4 nanoparticles coated with CPC.

structures of Fe-MNPs were not altered when coated with surfactant or exposed to Sb(V).

Surface structures of Fe-MNPs coated with surfactant were characterized by FT-IR spectra (Fig. 5). When compared with pure Fe-MNPs, adsorption peaks of $2920, 2850 \text{ cm}^{-1}$ in the spectrum of Fe-MNPs@CPC indicated the presence of vibrations of CH_2 and CH_3 in long chain alkanes. Adsorption bands of $570\text{--}635 \text{ cm}^{-1}$ were in accordance with vibration of $\text{Fe}\text{--}\text{O}$ (Shen et al., 2009). The peaks at 3400 cm^{-1} could represent stretching vibrations of amino groups in the hydrolysate of CPC (Wang et al., 2010). These observed peaks indicated that CPC was anchored on the surface of magnetic particles successfully.

Weakened adsorption peaks observed at 2915 and 2850 cm^{-1} were assigned to stretching vibrations of symmetry and antisymmetry CH_2 in long chain alkanes under acidic conditions. The intensity of this band after coating with Sb(V) was decreased, which indicated that Sb(V) removal may due to binding with $\text{--}\text{CH}_2$ moieties of CPC. Another FT-IR spectrum was observed when synthesized Fe_3O_4 nanoparticles were exposed to Sb(V) under acidic conditions. In alkaline conditions, adsorption peaks were altered significantly compared with those under acidic conditions, which implied removal of Sb(V) under alkaline conditions presented difference with that in acidic conditions.

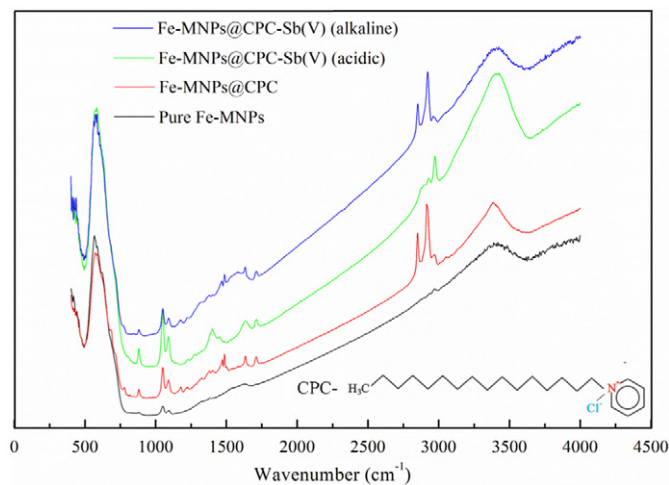


Fig. 5. FT-IR spectra of pure Fe-MNPs, Fe-MNPs@CPC and Fe-MNPs@CPC loaded with Sb(V) under acidic or alkaline conditions. (temperature: $25 \pm 1 \text{ }^\circ\text{C}$, the chemical structure of CPC was in bottom right corner).

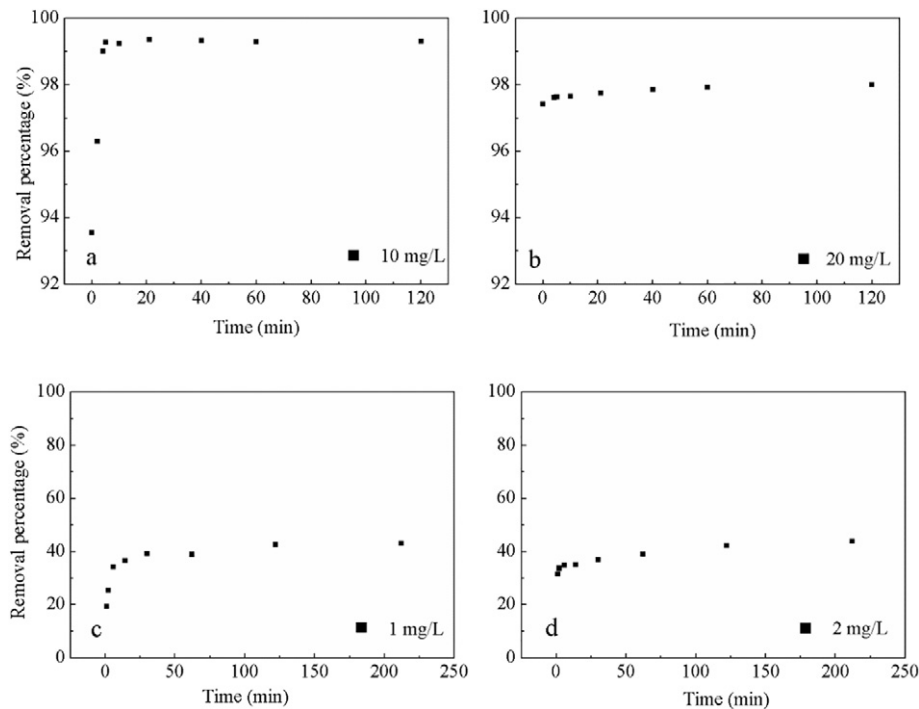


Fig. 6. Kinetics of Sb(V) adsorption on Fe-MNPs@CPC with different Sb(V) concentrations. Initial adsorbent concentration: 0.4 g/L. Acidic condition in (a) and (b), alkaline condition in (c) and (d). Temperature: 25 ± 1 °C.

3.2.2. Adsorption kinetics

Kinetics of Sb(V) on Fe-MNPs@CPC under acidic conditions showed that the adsorption percentage reached a plateau of 99–100% (10 mg/L) and 97–98% (20 mg/L) within approximately 10–40 min (Fig. 6a and Fig. 6b). Alternatively, adsorption reached steady state in less than 60 min under alkaline conditions (Fig. 6c and Fig. 6d). Thus, a contact time of 60 min was used in this study.

To describe adsorption kinetics of Sb(V), pseudo-first-order (PFO) (Eq. (1)) and pseudo-second-order (PSO) (Eq. (2)) models were applied.

$$\ln(q_e - q_t) = \ln q_e - k_1 t \quad (1)$$

$$\frac{t}{q_t} = \frac{1}{k_2 q_e^2} + \frac{t}{q_e} \quad (2)$$

where: q_e and q_t are the amounts of Sb(V) adsorbed on the Fe-MNPs at chemical equilibrium and time of t , respectively. K_1 (min^{-1}) and K_2 ($\text{g} \cdot \text{mg}^{-1} \cdot \text{min}^{-1}$) are the adsorption rate constants for the models (Eq. (1)) and (Eq. (2)), respectively.

Parameters of kinetic models that described conditions under acid or alkaline conditions were presented in Table S1. Correlation coefficients of models showed that PSO kinetic model was fitting well to simulate the adsorption of Sb(V) with contact time, which implied that adsorption might involve chemisorption between adsorbents and contaminants according to previous studies (Gücek et al., 2005; Ramesh et al., 2007). PSO rate constants (K) under acidic conditions were greater than that under alkaline conditions, which indicated higher adsorption rate constant under lower pH conditions than alkaline condition.

3.2.3. Adsorption isotherms

Initial Sb(V) concentrations ranged from 10 to 25 mg/L (acidic condition), 2 to 10 mg/L (alkaline conditions) and 0.4 g/L Fe-MNPs@CPC were dosed into solutions to evaluate adsorption performance as a function of Sb(V) concentrations. Adsorption isotherms of Sb(V) in acidic and alkaline conditions were presented in Table 1. Data used to derive adsorption isotherms were fitted by use of both Langmuir (3) and

Freundlich (4) models.

$$q_e = \frac{q_m K_L C_e}{1 + K_L C_e} \leftrightarrow \frac{C_e}{q_e} = \frac{1}{q_m K_L} + \frac{C_e}{q_m} \quad (3)$$

$$q_e = K_F C_e^{1/n} \leftrightarrow \lg q_e = \lg K_F + \frac{1}{n} \lg C_e \quad (4)$$

where: C_e (mg/L) is equilibrium concentration of Sb(V) in removal system, q_e is equilibrium adsorption amount (mg/g), q_m is the maximum adsorption capacity of the adsorbents. K_L and K_F are sorption affinity coefficients for Langmuir and Freundlich models, respectively.

The parameters derived by fitting isotherm models showed that Freundlich models, in which coefficients of determination (r^2) were greater than 0.97 (Fig. S4) were better fits for experimental adsorption data. This result might indicate that the heterogeneous surface energies by a multilayer adsorption could be used to describe adsorption behavior of Sb(V) on Fe-MNPs@CPC, and similar fitting results were also observed previously for perchlorate by granular activated carbon coated with surfactant (Xu et al., 2011). Adsorption efficiency of Fe-MNPs@CPC was higher than other adsorbents, for instance, the adsorption capacity of Fe-MNPs@CPC of 56.8 mg/g (25 mg Sb(V)/L was added in solution) was greater than that of bentonite ($Q_m = 0.556$ mg/g) (Xi et al., 2011), ferric hydroxide ($Q_m = 18.5$ mg/g) (Li et al., 2012), and polyvinyl alcohol-stabilized granular adsorbent containing nanoscale zero-valent iron ($Q_m = 1.65$ mg/g) (Zhao et al., 2014). This adsorption efficiency was lower than that of α -MnO₂ nanofibers ($Q_m = 89.99$ mg/g) (Luo et al., 2017) and zirconium oxide (ZrO₂)-carbon

Table 1

Parameters of Freundlich models of Sb(V) adsorption. Temperature: 25 ± 1 °C.

	Langmuir			Freundlich		
	K_L (L/mg)	Q_m (mg/g)	r^2	K_F ($\text{mg}^{1-(1/n)}\text{L}^{1/n}\text{g}^{-1}$)	n	r^2
Acidic	0.475	113.63	0.93	0.13	1.23	0.97
Alkaline	0.070	64.10	0.94	1.14	1.01	0.99

Table 2

Effects of coexisting matters on Sb(V) removal by Fe-MNPs@CPC in acidic condition. Adsorbent dosage: 0.4 g/L, Sb(V) concentration of 20 mg/L.

HA (mg/L)	Removal rate (HA)	Nitrate (mg/L)	Removal rate (NO ₃ ⁻)	Sulfate (mg/L)	Removal rate(SO ₄ ²⁻)	Phosphate (mg/L)	Removal rate (PO ₄ ³⁻)
10	93.2%	20	91.5%	10	91.4%	4	79.2%
20	93.0%	40	90.8%	20	94.2%	6	76.6%
30	92.8%	60	89.6%	30	95.7%	8	73.1%
40	91.1%	80	89.8%	40	95.4%	10	71.2%

nanofibers ($Q_m = 57.17$ mg/g) (Luo et al., 2015), but the cost of Fe-MNPs@CPC in this study was less than these materials.

3.2.4. Effect of external matters

The influence of several major coexisting matters in real waters, including humic acid (HA), nitrate, sulfate and phosphate on Sb(V) removal by Fe-MNPs@CPC were evaluated (Table 2). Amounts of HA and coexisting anions added were consistent with concentrations observed in surface waters (Guo et al., 2018; Zhu et al., 2009). In the presence of HA (10–40 mg/L), nitrate (20–80 mg/L) and sulfate (10–40 mg/L), removal rates of Sb(V) were approximately 90% (Table 2), which indicated that adsorption of Fe-MNPs@CPC was not inhibited by either humic acids or coexisting ions at environmentally relevant concentrations in surface waters.

As for phosphate, results of previous studies have revealed that the similar chemical properties of phosphorus and Sb could result to competition for adsorption sites on surfaces of adsorbents. When polyvinyl alcohol-stabilized granular adsorbent containing nanoscale zero-valent iron was utilized to remove Sb(V), a similar inhibiting effect of 5 mg/L phosphate resulted a 40% decreased in proportion of Sb(V) removed (Zhao et al., 2014). The presence of phosphate also decreased the proportion of As(V) removed by sorption of mixed magnetite-maghemite nanoparticles to 30% (Chowdhury and Yanful, 2010). In this study, results of which are presented here, addition of phosphate (4–10 mg/L) inhibited adsorption of Sb(V) by Fe-MNPs@CPC to 70–80% of maximum. But it's should be noted that concentrations of phosphate detected in most of surface waters were significantly lower than the concentrations added during this study (4–10 mg/L) (Liu et al., 2010; Zhu et al., 2009). Even in the presence of 10 mg PO₄³⁻/L, adsorption capacity of Fe-MNPs@CPC was 35.6 mg Sb(V)/g.

3.2.5. Application to removal of Sb(V) from typical contaminated waters

Application of adsorbent in real contaminated waters, which was more complicated than simple synthetic waters for the presence of various kinds of ions and organic matters, could confirm practical application of adsorbent in real waters. The physicochemical characteristics of contaminated waters were presented in Table S2.

The removal rates of synthesized adsorbents in typical real waters were shown in Table 3. In the paddy field water, only 93.04% Sb(V) was removed by Fe-MNPs@CPC, which due to a relatively large concentration of PO₄³⁻ (25.23 mg/L) that could compete with Sb(V) for adsorption sites. In general, removal rates of Sb(V) by Fe-MNPs@CPC were

Table 3

Removal of Fe-MNPs@CPC from various types of surface waters. Initial adsorbents dosage: 0.4 g/L, pH: 5.0 ± 0.1.

Types	Concentration of Sb(V) (μg/L)	Residual concentrations (μg/L)	Removal rate (%)
Paddy field water	154.85	10.78	93.04
Reservoir water	227.50	1.60	99.30
Tap water	254.72	1.89	99.26
Retained water	2286.08	27.78	98.78
Well water	153.95	0.44	99.71

>90% in various types waters, especially 99.71% removal rate in well water (Table 3). The elevated concentrations of Sb(V) could be adsorbed to relatively low concentrations, for instance, a concentration of 2286.08 μg/L Sb(V) was reduced to 27.78 μg/L. The application indicated that Fe-MNPs coated with CPC could be performed as a highly-efficient adsorbent for Sb(V) removal from real contaminated waters.

3.2.6. Regeneration and reuse of adsorbents

Decreasing removal performance of Sb(V) when pH greater than 7 indicated that alkaline conditions may favor desorption of Sb(V). Therefore, deionized water, various concentrations of NaOH and metal chelating agent, EDTA-2Na, were tested to evaluate their desorption ability on Sb removal during regeneration of adsorbents.

Adsorption of Sb(V) after several consecutive adsorption/desorption cycles, with deionized water, NaOH solutions (0.5 M, 1.0 M, 2.0 M) or EDTA-2Na (0.075 M, 0.15 M, 0.3 M) were presented in Fig. 7. Desorption ability of these solvents in increasing order were: deionized water < EDTA-2Na < NaOH. Take the fifth adsorption/desorption cycle as example, the Sb(V) removal performance of Fe-MNPs@CPC after desorption with 0.5 M NaOH, 1.0 M NaOH and 2.0 M NaOH reached 71.2%, 91.2% and 92.3%, this adsorption ability was superior to deionized water (51.2%), 0.075 M EDTA-2Na(83.0%), 0.15 M EDTA-2Na(71.0%) and 0.3 M EDTA-2Na(56.1%). Moreover, both 1.0 and 2.0 M NaOH resulted in relatively high removal rates of ~90% than did 71.2% of 0.5 M NaOH solution during fifth cycles, which indicated that 1.0 M NaOH was an efficient solution for regeneration of adsorbent. In the presence of 0.5, 1 and 2 M NaOH, the pH of solutions could reach 13.7, 14 and 14.3, with high concentrations of OH⁻ that several orders of magnitude greater than solutions of pH 8–12. This high content of OH⁻ could replace with Sb(V) that removed via the electrostatic attraction with CP⁺ (dissociated from CPC). It is worth noting that adsorption performance of Sb(V) decreased slightly after each consecutive cycle, which can be attributed to irreversible adsorption of Sb(V) on core Fe-MNPs (Mayo et al., 2007). Compared with the TEM image and magnetization

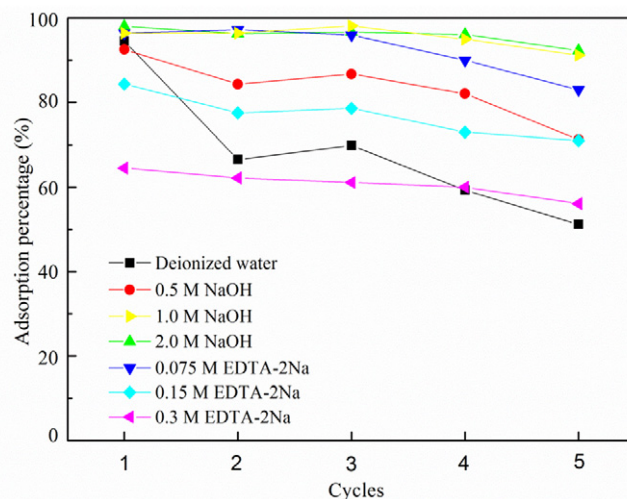
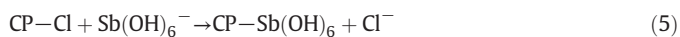


Fig. 7. Adsorption of Sb(V) during five consecutive adsorption/desorption cycles. Initial adsorbent concentration: 0.4 g/L; Sb(V) concentration: 1 mg/L; temperature: 25 ± 1 °C.

curves of synthesized Fe-MNPs@CPC in Fig. 4b and d, mean sizes of Fe-MNPs@CPC after five regeneration cycles were not altered significantly and saturation magnetization reached 42.2 emu/g. This dispersibility and superparamagnetic property still met the requirements of Sb(V) removal in aqueous solutions (Fig. S5). The regeneration experiments clearly showed that Fe-MNPs coated with surfactant could be used repeatedly several times with relatively high removal ability.

3.3. Mechanism of Sb(V) removal with introduction of surfactant

Previous studies have suggested that adsorption of ionic contaminants was achieved by electrostatic interactions, ion exchange and surface complexation (Lv, 2007; Xu et al., 2011). In this study, the deprotonated hydroxyl groups ($-\text{OH}$) in Fe-MNPs surface could bond with one or two layers of CPC and forming surfactant monolayer and surfactant bilayer respectively. In the process of mixed hemimicelles, CP^+ (dissociated from CPC) in the outer layer of surfactant bilayers were responsible for $\text{Sb}(\text{V})(\text{Sb}(\text{OH})_6^-)$ adsorption and forming outer-sphere complexation via electrostatic attraction. As a result, higher zeta potential of Fe-MNPs@CPC favored Sb(V) removal in acidic condition as presented in Fig. S1. Characterization analysis results also supported this conclusion, the percentage of atomic contents in XPS analyses showed that contents of chlorine (Cl) decreased sharply when Sb(V) was adsorbed on surfaces of Fe-MNPs@CPC in Table S3. The process of Sb(V) removal in the surface of adsorbent can be expressed as Eq. (5).



On the other hand, Sb(V) removal was not improved as pH decreased below than 3. This result implied that electrostatic attraction was not the only mechanism of Sb(V) removal by Fe-MNPs coated with surfactant. Sb $3d_{3/2}$ peaks in XPS spectra (Fig. 2) where Sb(V) was adsorbed to Fe-MNPs@CPC indicated surface chemical bonding with deprotonated $-\text{OH}$ groups were in part responsible for Sb(V) removal, and forming stable inner-sphere complexation. Removal rates of reused adsorbent decreasing in consecutive regeneration cycles also indicated that Sb(V) bond with surface of core Fe-MNPs. Another characterization result of FT-IR spectra showed that the adsorption peaks of CH_2 in long chain alkanes decreased after removal process, that indicated that Sb(V) removal may occur in CH_2 of long chain

alkanes. Thus, surface bonding that occurred in CH_2 of long chain alkanes and core of Fe-MNPs may serve another important role in Sb(V) removal apart from electrostatic force. Furthermore, electrostatic attraction might serve a weaker role under alkaline conditions for the decreasing zeta potential of adsorbent in higher pH condition (Fig. S1).

Overall, electrostatic attraction and surface bonding were involved into adsorption of Sb(V) by Fe-MNPs coated with cationic surfactant. The removal mechanisms and possible binding sites were exhibited in Fig. 8.

4. Conclusions

In this study, the adsorbent of Fe-MNPs coated with CPC has a better performance in Sb(V) removal than Fe-MNPs@CTAB and pure Fe-MNPs, thus CPC was selected as synthesized modifier; optimal mass ratio of Fe-MNPs and CPC as 4:1 and pH in 3–5 were obtained to gain efficient removal performance. When CPC was introduced, magnetic properties or crystalline structure of adsorbent were not altered significantly, and its dispersibility was enhanced; this efficient adsorbent exhibited its low cost but better removal ability of Sb(V) than other adsorbents; the removal percentile of >90% using Fe-MNPs@CPC were achieved in real contaminated water further confirmed its practicability; 1 M NaOH was selected as desorbent for Sb(V) removal in consecutive regeneration cycle. Abovementioned experiment results and different characterization analyses suggested that electrostatic attraction and surface bonding contribute the removal process of Sb(V) by Fe-MNPs after modification of cationic surfactant. The synthesized Fe-MNPs@CPC could be proved as an effective, recycled and easy separation adsorbent for Sb(V) and other anionic contaminants from water.

Declaration of competing interest

The author declare that they have no known competing interests or personal relationships that could have appeared to influence the work reported in this paper.

Acknowledgements

This research was supported by the National Natural Science Foundation of China (41473109) and the Ministry of Science and Technology of the People's Republic of China (No. 2017ZX07301005).

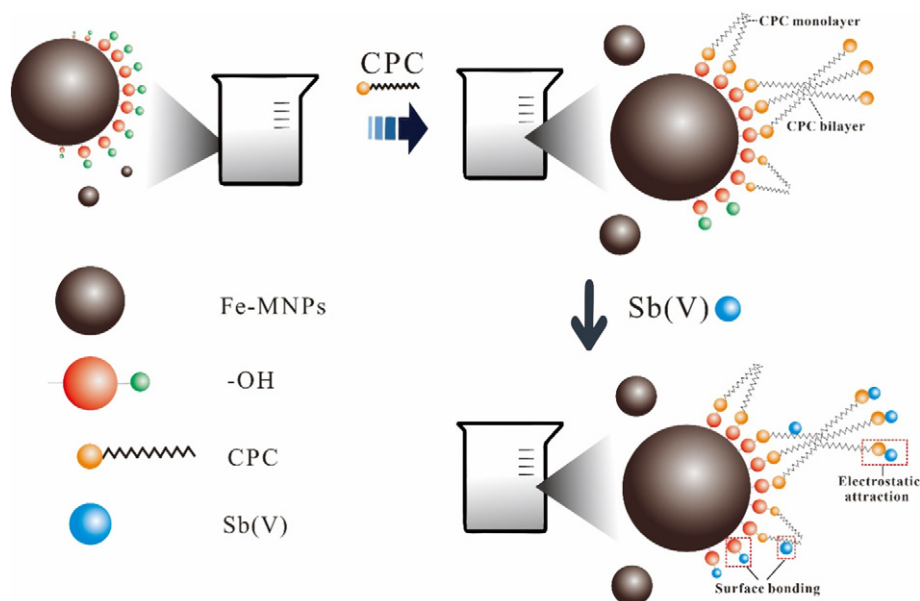


Fig. 8. Possible removal mechanisms of Sb by Fe-MNPs coated with cationic surfactant.

Appendix A. Supplementary data

Supplementary data to this article can be found online at <https://doi.org/10.1016/j.scitotenv.2019.136302>.

References

- Amarasiriwardena, D., Wu, F., 2011. Antimony: emerging toxic contaminant in the environment. *Microchem. J.* 97 (1), 1–3.
- Atkin, R., Craig, V.S.J., Wanless, E.J., Biggs, S., 2003. Mechanism of cationic surfactant adsorption at the solid–aqueous interface. *Adv. Colloid Interf. Sci.* 103 (3), 219–304.
- Chen, W.F., Zhang, Z.Y., Li, Q., Wang, H.Y., 2012. Adsorption of bromate and competition from oxyanions on cationic surfactant-modified granular activated carbon (GAC). *Chem. Eng. J.* 203 (5), 319–325.
- Chowdhury, S.R., Yanful, E.K., 2010. Arsenic and chromium removal by mixed magnetite–maghemite nanoparticles and the effect of phosphate on removal. *J. Environ. Manag.* 91 (11), 2238–2247.
- EU, 1976. Council Directive 76/464/EEC of 4 May 1976 on pollution caused by certain dangerous substances discharged into the aquatic environment of the community. *Off. J. L* 129, 23–29.
- Feng, L., Cao, M., Ma, X., Zhu, Y., Hu, C., 2012. Superparamagnetic high-surface-area Fe₃O₄ nanoparticles as adsorbents for arsenic removal. *J. Hazard. Mater.* 217–218, 439–446.
- Filella, M., Belzile, N., Chen, Y.-W., 2002a. Antimony in the environment: a review focused on natural waters: I. occurrence. *Earth-Sci. Rev.* 57 (1), 125–176.
- Filella, M., Belzile, N., Chen, Y.-W., 2002b. Antimony in the environment: a review focused on natural waters: II. Relevant solution chemistry. *Earth-Sci. Rev.* 59 (1), 265–285.
- Fu, Z., Wu, F., Amarasiriwardena, D., Mo, C., Liu, B., Zhu, J., Deng, Q., Liao, H., 2010. Antimony, arsenic and mercury in the aquatic environment and fish in a large antimony mining area in Hunan, China. *Sci. Total Environ.* 408 (16), 3403–3410.
- Gebel, T., Christensen, S., Dunkelberg, H., 1997. Comparative and environmental genotoxicity of antimony and arsenic. *Anticancer Res.* 17 (4A), 2603–2607.
- Grossi, P.R., Eick, M., Sparks, D.L., Goldberg, S., Ainsworth, C.C., 1997. Arsenate and chromate retention mechanisms on goethite. 2. Kinetic evaluation using a pressure-jump relaxation technique. *Environ. Sci. Technol.* 31, 321–326.
- Gücek, A., Şener, S., Bilgen, S., Mazmanç, M.A., 2005. Adsorption and kinetic studies of cationic and anionic dyes on pyrophyllite from aqueous solutions. *J. Colloid Interface Sci.* 286, 53–60.
- Guo, J., Su, L., Zhao, X., Xu, Z., Chen, G., 2016. Relationships between urinary antimony levels and both mortalities and prevalence of cancers and heart diseases in general US population, NHANES 1999–2010. *Sci. Total Environ.* 571, 452–460.
- Guo, W., Fu, Z., Wang, H., Song, F., Wu, F., Giesy, J.P., 2018. Environmental geochemical and spatial/temporal behavior of total and speciation of antimony in typical contaminated aquatic environment from Xikuangshan, China. *Microchem. J.* 137, 181–189.
- Guo, X., Wu, Z., He, M., 2009. Removal of antimony (V) and antimony (III) from drinking water by coagulation–flocculation–sedimentation (CFS). *Water Res.* 43 (17), 4327–4335.
- Guo, X., Wu, Z., He, M., Meng, X., Jin, X., Qiu, N., Zhang, J., 2014. Adsorption of antimony onto iron oxyhydroxides: adsorption behavior and surface structure. *J. Hazard. Mater.* 276, 339–345.
- Hammel, W., Debus, R., Steubing, L., 2000. Mobility of antimony in soil and its availability to plants. *Chemosphere* 41 (11), 1791–1798.
- He, M., Wang, X., Wu, F., Fu, Z., 2012. Antimony pollution in China. *Sci. Total Environ.* 421, 41–50.
- Jin, Y., Liu, F., Tong, M., Hou, Y., 2012. Removal of arsenate by cetyltrimethylammonium bromide modified magnetic nanoparticles. *J. Hazard. Mater.* 227–228, 461–468.
- Kang, M., Kawasaki, M., Tamada, S., Kamei, T., Magara, Y., 2000. Effect of pH on the removal of arsenic and antimony using reverse osmosis membranes. *Desalination* 131 (1), 293–298.
- Kong, L., He, M., Hu, X., 2016. Rapid photooxidation of Sb (III) in the presence of different Fe (III) species. *Geochim. Cosmochim. Acta* 180, 214–226.
- Leng, Y., Guo, W., Su, S., Yi, C., Xing, L., 2012. Removal of antimony(III) from aqueous solution by graphene as an adsorbent. *Chem. Eng. J.* 211–212, 406–411.
- Leuz, A.-K., Johnson, C.A., 2005. Oxidation of Sb (III) to Sb (V) by O₂ and H₂O₂ in aqueous solutions. *Geochim. Cosmochim. Acta* 69 (5), 1165–1172.
- Li, N., Zhang, L., Chen, Y., Tian, Y., Wang, H., 2011. Adsorption behavior of Cu(II) onto titanate nanofibers prepared by alkali treatment. *J. Hazard. Mater.* 189, 265–272.
- Li, X., Dou, X., Li, J., 2012. Antimony(V) removal from water by iron–zirconium bimetal oxide: performance and mechanism. *J. Environ. Sci.* 24 (7), 1197–1203.
- Lin, S., Lu, D., Liu, Z., 2012. Removal of arsenic contaminants with magnetic γ-Fe₂O₃ nanoparticles. *Chem. Eng. J.* 211–212, 46–52.
- Liu, F., Le, X.C., McKnight-Whitford, A., Xia, Y., Wu, F., Elswick, E., Johnson, C.C., Zhu, C., 2010. Antimony speciation and contamination of waters in the Xikuangshan antimony mining and smelting area, China. *Environ. Geochem. Health* 32 (5), 401–413.
- Luo, J., Luo, X., Crittenden, J., Qu, J., Bai, Y., Peng, Y., Li, J., 2015. Removal of antimonite (Sb (III)) and antimonate (Sb (V)) from aqueous solution using carbon nanofibers that are decorated with zirconium oxide (ZrO₂). *Environ. Sci. Technol.* 49 (18), 11115–11124.
- Luo, J., Hu, C., Meng, X., Crittenden, J., Qu, J., Peng, P., 2017. Antimony removal from aqueous solution using novel α-MnO₂ nanofibers: equilibrium, kinetic and DFT studies. *ACS Sustain. Chem. Eng.* 5 (3), 2255–2264.
- Lv, L., 2007. Defluoridation of drinking water by calcined MgAl-CO₃ layered double hydroxides. *Desalination* 208, 125–133.
- Mayo, J.T., Yavuz, C., Yean, S., Cong, L., Shipley, H., Yu, W., Falkner, J., Kan, A., Tomson, M., Colvin, V.L., 2007. The effect of nanocrystalline magnetite size on arsenic removal. *Sci. Technol. Adv. Mat.* 8 (1–2), 71–75.
- Poon, R., Chu, I., Lecavalier, P., Valli, V., Foster, W., Gupta, S., Thomas, B., 1998. Effects of antimony on rats following 90-day exposure via drinking water. *Food Chem. Toxicol.* 36 (1), 21–35.
- Ramesh, A., Hasegawa, H., Maki, T., Ueda, K., 2007. Adsorption of inorganic and organic arsenic from aqueous solutions by polymeric Al/Fe modified montmorillonite. *Sep. Purif. Technol.* 56 (1), 90–100.
- SAC (Standardization Administration of the People’s Republic of China), 2002i. Standards for Surface Water Quality, GB-3838-2002.
- Shen, Y.F., Tang, J., Nie, Z.H., Wang, Y.D., Ren, Y., Zuo, L., 2009. Tailoring size and structural distortion of Fe₃O₄ nanoparticles for the purification of contaminated water. *Bioresour. Technol.* 100 (18), 4139–4146.
- Song, P., Song, Q., Yang, Z., Zeng, G., Xu, H., Li, X., Xiong, W., 2018. Numerical simulation and exploration of electrocoagulation process for arsenic and antimony removal: electric field, flow field, and mass transfer studies. *J. Environ. Manag.* 228, 336–345.
- Sun, X., Zheng, C., Zhang, F., Li, L., Yang, Y., Wu, G., Guan, N., 2008. β-Cyclodextrin-assisted synthesis of superparamagnetic magnetite nanoparticles from a single Fe (III) precursor. *J. Phys. Chem. C* 112, 17148–17155.
- Sundar, S., Chakravarty, J., 2010. Antimony toxicity. *Int. J. Environ. Res. Public Health* 7 (12), 4267–4277.
- Tie, S.L., Lin, Y.Q., Lee, H.C., Bae, Y.S., Lee, C.H., 2006. Amino acid-coated nano-sized magnetite particles prepared by two-step transformation. *Colloid Surface A* 273 (1–3), 75–83.
- Ungureanu, G., Santos, S., Boaventura, R., Botelho, C., 2015. Arsenic and antimony in water and wastewater: overview of removal techniques with special reference to latest advances in adsorption. *J. Environ. Manag.* 151, 326–342.
- USEPA, 1979. Water Related Fate of the 129 Priority Pollutants. vol. 1. USEPA, Washington, DC, USA.
- Van Velzen, D., 1998. Antimony, its sources, applications and flow paths into urban and industrial waste : a review. *Waste Manage. Res.* 16 (1), 32–40.
- Vithanage, M., Rajapaksha, A.U., Ahmad, M., Uchimiya, M., Dou, X., Alessi, D.S., Ok, Y.S., 2015. Mechanisms of antimony adsorption onto soybean Stover-derived biochar in aqueous solutions. *J. Environ. Manag.* 151, 443–449.
- Wang, J., Zheng, S., Yun, S., Liu, J., Xu, Z., Zhu, D., 2010. Amino-functionalized Fe₃O₄@SiO₂ core–shell magnetic nanomaterial as a novel adsorbent for aqueous heavy metals removal. *J. Colloid Interface Sci.* 349 (1), 293–299.
- Wang, Z., Guo, H., Yu, Y., He, N., 2006. Synthesis and characterization of a novel magnetic carrier with its composition of Fe₃O₄/carbon using hydrothermal reaction. *J. Magn. Mater.* 302 (2), 397–404.
- Watanabe, N., Inoue, S., Ito, H., 1999. Antimony in municipal waste. *Chemosphere* 39 (10), 1689–1698.
- White, B.R., Stackhouse, B.T., Holcombe, J.A., 2009. Magnetic gamma-Fe(2)O(3) nanoparticles coated with poly-L-cysteine for chelation of as(III), cu(II), cd(II), Ni(II), Pb(II) and Zn(II). *J. Hazard. Mater.* 161 (2–3), 848–853.
- Wu, F., Fu, Z., Liu, B., Mo, C., Chen, B., Corns, W., Liao, H., 2011. Health risk associated with dietary co-exposure to high levels of antimony and arsenic in the world’s largest antimony mine area. *Sci. Total Environ.* 409, 3344–3351.
- Wu, F., Sun, F., Wu, S., Yan, Y., Xing, B., 2012. Removal of antimony (III) from aqueous solution by freshwater cyanobacteria *Microcystis* biomass. *Chem. Eng. J.* 183, 172–179.
- Wu, Z., He, M., Guo, X., Zhou, R., 2010. Removal of antimony (III) and antimony (V) from drinking water by ferric chloride coagulation: competing ion effect and the mechanism analysis. *Sep. Purif. Technol.* 76 (2), 184–190.
- Xi, J., He, M., Lin, C., 2011. Adsorption of antimony (III) and antimony (V) on bentonite: kinetics, thermodynamics and anion competition. *Microchem. J.* 97 (1), 85–91.
- Xu, J.H., Gao, N.Y., Deng, Y., Sui, M.H., Tang, Y.L., 2011. Perchlorate removal by granular activated carbon coated with cetyltrimethyl ammonium bromide. *J. Colloid Interface Sci.* 357 (2), 474–479.
- Zhao, X., Shi, Y., Cai, Y., Mou, S., 2008. Cetyltrimethylammonium bromide-coated magnetic nanoparticles for the preconcentration of phenolic compounds from environmental water samples. *Environ. Sci. Technol.* 42 (4), 1201–1206.
- Zhao, X., Dou, X., Mohan, D., Pittman, C.U., Ok, Y.S., Jin, X., 2014. Antimonate and antimonite adsorption by a polyvinyl alcohol-stabilized granular adsorbent containing nanoscale zero-valent iron. *Chem. Eng. J.* 247 (7), 250–257.
- Zhu, J., Wu, F., Deng, Q., Shao, S., Mo, C., Pan, X., Li, W., Zhang, R., 2009. Environmental characteristics of water near the Xikuangshan antimony mine, Hunan Province. *Acta Sci. Circum.* 29 (2), 655–661.
- Zhu, J., Wu, F., Pan, X., Guo, J., Wen, D., 2011. Removal of antimony from antimony mine flotation wastewater by electrocoagulation with aluminum electrodes. *J. Environ. Sci.* 23 (7), 1066–1071.
- Zou, J.-P., Liu, H.-L., Luo, J., Xing, Q.-J., Du, H.-M., Jiang, X.-H., Luo, X.-B., Luo, S.-L., Suib, S.L., 2016. Three-dimensional reduced Graphene oxide coupled with Mn₃O₄ for highly efficient removal of Sb (III) and Sb (V) from water. *ACS Appl. Mater. Inter.* 8 (28), 18140–18149.

Synthesis of Fe₃O₄ magnetic nanoparticles coated with cationic surfactants and their applications in Sb(V) removal from water

Wenjing Guo ^{a,b}, Zhiyou Fu ^{a*}, Zhiyong Zhang ^b, Hao Wang ^c, Shasha Liu ^a, Weiying Feng ^a, Xiaoli Zhao ^a, John P. Giesy ^{a,d}

^a *State Key Laboratory of Environment Criteria and Risk Assessment, Chinese Research Academy of Environmental Sciences, Beijing 100012, China*

^b *Institute of Agricultural Resource and Environmental Sciences, Jiangsu Academy of Agricultural Sciences, Nanjing 210014, China*

^c *South China Institute of Environmental Sciences, Ministry of Environmental Protection, Guangzhou 510655, China*

^d *Department of Biomedical and Veterinary Biosciences and Toxicology Centre, University of Saskatchewan, Saskatoon, Saskatchewan, Canada*

* *Corresponding author: Zhiyou Fu, zhiyoufu@126.com. +86-10-84915312*

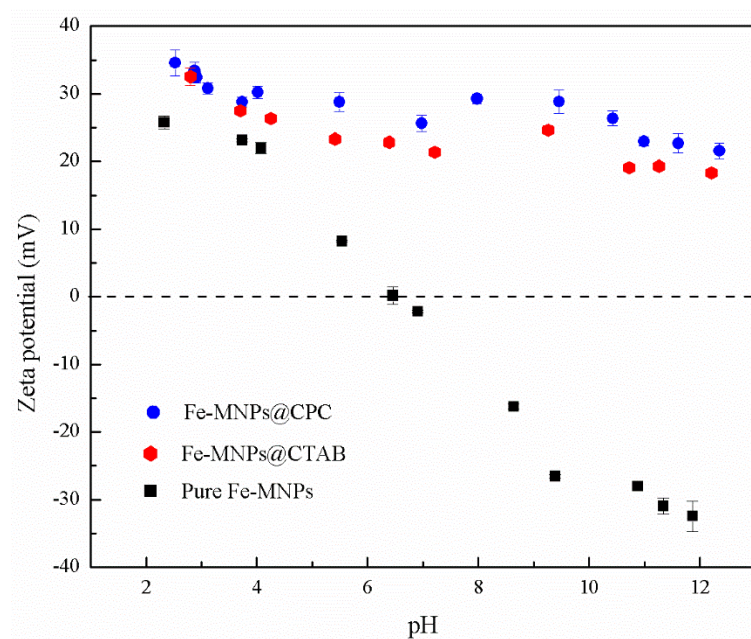


Fig. S1. Zeta potentials of Fe-MNPs@CPC, Fe-MNPs@CTAB and pure Fe-MNPs in the range of pH 2-12. (Initial adsorbent concentration: 0.4 g/L; temperature: 25 ± 1 °C)

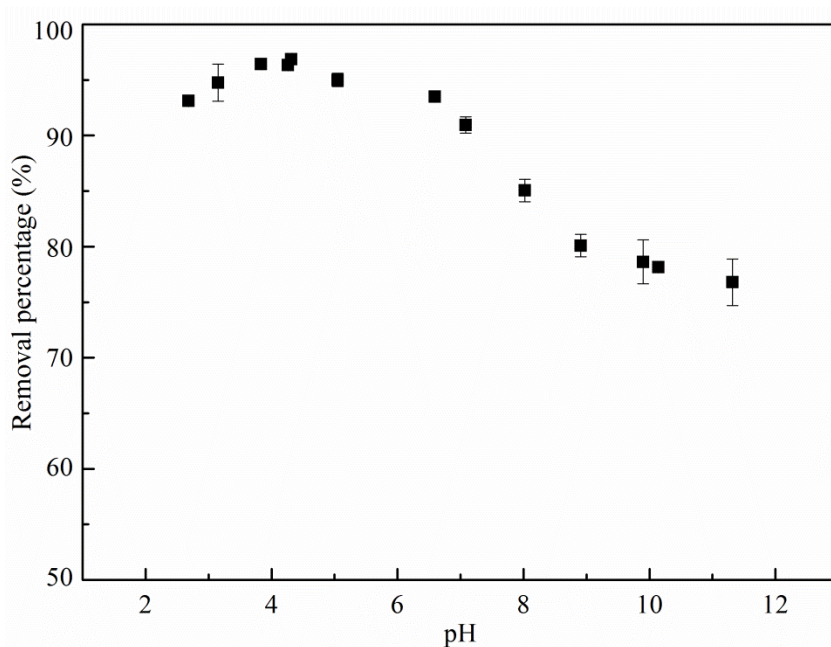


Fig. S2. Effect of pH on the Sb(V) removal percentages from an aqueous solution containing an initial concentration of 2 mg/L Sb(V) and 0.4 g/L of adsorbent.

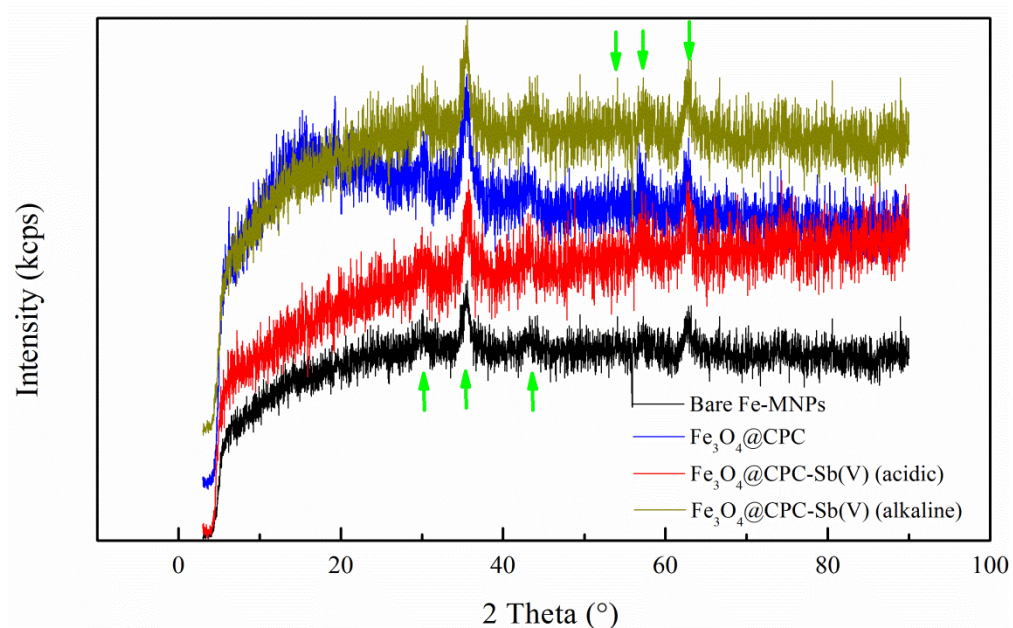


Fig. S3. XRD patterns of bare Fe-MNPs, Fe-MNPs@CPC, and Fe-MNPs@CPC loaded with Sb(V) under acidic and alkaline conditions.

Table S1 Parameters of the pseudo-second-order kinetic model for the adsorption of Sb(V).

Sb(V) concentration	pseudo-second-order (PSO)		
	q_e (mg·g ⁻¹)	k_2 (g·mg ⁻¹ ·min ⁻¹)	r^2
10 ppm	24.81	2.71	0.98
Acidic conditions			
20 ppm	49.02	0.35	0.99
1 ppm	1.09	0.178	0.99
Alkaline conditions			
2 ppm	2.04	0.20	0.98

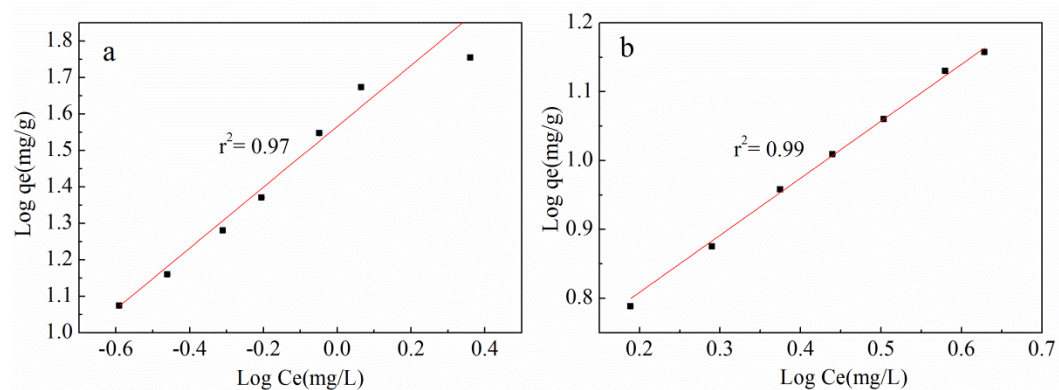


Fig. S4. Freundlich models of Sb(V) adsorption by Fe-MNPs@CPC under (a) acidic and (b) alkaline conditions.

Table S2 Physicochemical characteristics of several typical contaminated waters in the vicinity of the XKS mine.

Types	Sb(V)($\mu\text{g/L}$)	pH	TOC(mg/L)	NO_3^- (mg/L)	PO_4^{3-} (mg/L)	SO_4^{2-} (mg/L)	Al($\mu\text{g/L}$)	Fe($\mu\text{g/L}$)	Mn($\mu\text{g/L}$)	Zn($\mu\text{g/L}$)
1	154.85	7.38	4.53	1.31	25.23	5.80	32.33	43.92	0.55	1094.51
2	227.5	7.65	1.64	2.48	1.87	36.68	52.52	46.67	0.46	1289.46
3	254.72	6.63	1.48	7.37	0.0721	38.48	54.16	59.35	1.34	1269.99
4	2286.08	6.75	3.4	3.02	0.087	43.48	27.71	74.62	1.31	1164.63
5	153.95	7.57	0.319	4.72	0.82	80.84	25.26	74.74	1.41	1538.42

1-paddy field water, 2-reservoir water, 3-tap water, 4-retained water and 5-well

water, <LOD represented less than limit of detection.

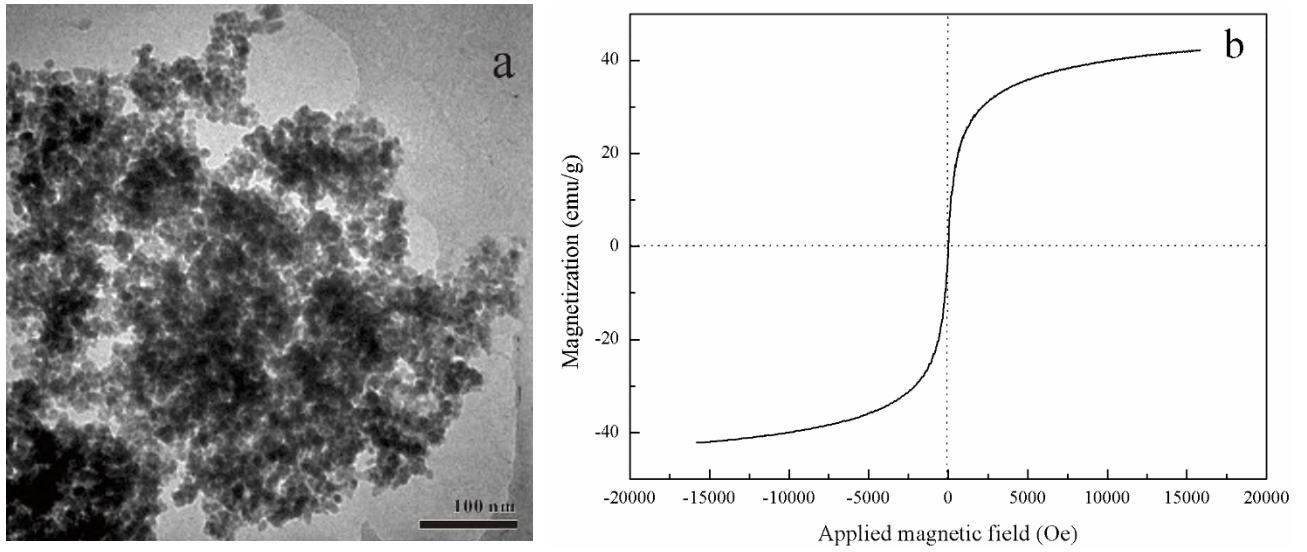


Fig. S5. (a) TEM images of Fe-MNPs after the fifth adsorption/desorption cycle;
 (b) Magnetization curves of Fe-MNPs@CPC after the fifth adsorption/desorption cycle.

Table S3 Mass percentage of atomic contents based on the XPS analyses.

	C 1s	N 1s	O 1s	Cl 2p	Fe 2p	Sb 3d
Pure Fe-MNPs	21.66	0.01	46.79	0.25	31.28	0.00
Fe-MNPs@CPC	72.85	2.98	14.91	2.15	7.12	0.00
Fe-MNPs@CPC-Sb(V) (acidic)	17.62	0.30	57.85	0.17	22.54	1.52
Fe-MNPs@CPC-Sb(V) (alkaline)	46.51	1.59	36.80	0.38	14.50	0.22
Fe-MNPs@CTAB-Sb(V) (acidic)	16.97	0.40	56.39	0.00	24.70	1.54
Fe-MNPs@CTAB-Sb(V) (alkaline)	38.86	0.99	38.84	0.00	21.30	0.01